Unjamming of active rotators

Linda Ravazzano [a], Silvia Bonfanti[a], Maria Chiara Lionetti[b], Maria Rita Fumagalli[b,c], Roberto Guerra[a], Oleksandr Chepizhko [d], Caterina A. M. La Porta [*,b,c,e], Stefano Zapperi[*,a,f],

Received Xth XXXXXXXXXX 20XX, Accepted Xth XXXXXXXXX 20XX
First published on the web Xth XXXXXXXXXX 200X
DOI: 10.1039/b000000x

Active particle assemblies can exhibit a wide range of interesting dynamical phases depending on internal parameters such as density, adhesion strength or self-propulsion. Active self-rotations are rarely studied in this context, although they can be relevant for active matter systems, as we illustrate by analyzing the motion of *Chlamydomonas reinhardtii* algae under different experimental conditions. Inspired by this example, we simulate the dynamics of a system of interacting active disks endowed with active torques and self-propulsive forces. At low packing fractions, adhesion causes the formation of small rotating clusters, resembling those observed when algae are stressed. At higher densities, the model shows a jamming to unjamming transition promoted by active torques and hindered by adhesion. We also study the interplay between self-propulsion and self-rotation and derive a phase diagram. Our results yield a comprehensive picture of the dynamics of active rotators, providing useful guidance to interpret experimental results in cellular systems where rotations might play a role.

1 Introduction

Recent years witnessed a growing interest in the properties of active matter, where the system is composed by self-propelled units[1,2]. The field was inspired by the observation of natural phenomena such as the movements of flocks of birds[3], schools of fishes or cell populations[4], and pushed forward by new technological achievements that allowed the production of active colloids[5], Janus particles[6] and artificial microswimmers[7]. Basic concepts of statistical physics have been applied to the study of ensembles of active particles in order to investigate not only single particle properties, but also their collective behavior[1,2]. Active matter has shown a rich variety of emerging phenomena, due to the fact that those systems are out of thermodynamical equilibrium[1,2]. Notable examples are the emergence of vortices in confined geometries[8], the formation of clusters[9] and active cristals[10], and phase transitions that differ from the ones typical of passive particles. For instance in active particle systems, the activity itself can induce phase separation[11] or phase coexistence between regions with hexatic order and regions in the liquid or gas phase[12].

Most theoretical studies of active matter consider self-propelled particles driven by active forces. The observation of biological active matter suggests, however, that active torques may also play an important and yet unexplored role. An interesting example is provided by *Chlamydomonas reinhardtii* (*C. reinhardtii*), a micron-sized unicellular alga that is able to move thanks to two flagella. It has been noticed that those organisms not only self-propel to perform translational motion, but they also have the ability to self-rotate. This peculiar behavior is due to the morphology of this alga, characterized by an éyespotśensible to light located near the cell equator. Rotating around its own axis the alga allows the eyespot to better scan the surrounding environment looking for light, needed to perform photosyntesis[13]. In this paper, we report observations and quantification of individual rotation and the formation of rotating clusters, in analogy to what observed for model systems of active rotating disks in 2D passive media[14].

Inspired by this biological example, we study the dynamic behavior of a collection of interacting active rotators in two dimensions. Our model system displays some analogies with chiral active fluids which are composed by particles spinning with a defined chirality and display peculiar physical properties such an odd (or Hall) viscosity due to breaking both parity and time-reversal symmetries[15] and the emergence of active turbulence behavior[16]. Another interesting example of rotating active particles was provided in Ref.[17] where the authors studied a set of 3D printed active spinner driven by air flow. The results showed diffusive behavior and non-equilibrium dynamical phases.

[a] *Center for Complexity and Biosystems, Department of Physics, University of Milano, via Celoria 26, 20133 Milano, Italy*
[b] *Center for Complexity and Biosystems, Department of Environmental Science and Policy, University of Milan, via Celoria 26, 20133 Milano, Italy*
[c] *CNR - Consiglio Nazionale delle Ricerche, Biophysics institute, via De Marini 6, Genova, Italy*
[d] *Institut für Theoretische Physik, Leopold-Franzens-Universität Innsbruck, Technikerstrasse 21a, A-6020 Innsbruck, Austria*
[e] *Innovation for Well-Being and Environment (CR-I-WE), University of Milan, Milan, Italy.*
[f] *CNR - Consiglio Nazionale delle Ricerche, Istituto di Chimica della Materia Condensata e di Tecnologie per l'Energia, Via R. Cozzi 53, 20125 Milano, Italy*
[*] Corresponding authors: caterina.laporta@unimi.it,stefano.zapperi@unimi.it

Here we focus on the jamming-unjamming transition displayed by a system of active rotators. This transition, typical of granular materials, shares some features with the glass transition. Increasing the density, the system goes from an unjammed liquid-like phase to a jammed solid-like state, characterized by limited mobility and slow relaxation[18]. Interestingly, this kind of transition has been observed to take place also in systems of living cells where it may play a role in biological processes, such as inside the epithelial tissues of patients affected by asthma[19] or in the migration of cancer cells during wound healing[20]. In this paper, we explore the role of self-rotation on the jamming-unjamming phase transition of a system of bidimensional disks, performing molecular dynamics simulations with LAMMPS (http://lammps.sandia.gov.)[21].

2 Materials and Methods

2.1 Experiments

2.1.1 ***C. reinhardtii*** **culture growth and exposure to stress conditions.** *C. reinhardtii* cells were growth in TAP medium (Invitrogen) as batch cultures until they reached $1-2\times10^6$ cells/ml (corresponding to mid-exponential phase of growth). The cells were cultured under continuous cool-white fluorescent lamps ($\simeq 100\mu$ mol photons/m^2 s) within a 110 rpm shaking incubator, at 25°C. For palmelloid analysis, 5 ml of cells was spun at 1100 g/5 min/25° C and resuspended in 20 ml of Tris-Acetate-Phosphate (TAP, Invitrogen cod. A1379801) medium containing 150 mM NaCl or in fresh TAP growth medium (control condition) for 6 hrs. 200 μl of cultured cells for each experimental condition were seeded in a 96 well and time-lapse imaged immediately. For study of motility at different densities, 200 μl of cultured cells ($2\cdot10^6$ cells/ml and 10^6 cells/ml respectively) were let sediment on the bottom of a 96 well before imaging. Images were acquired with DMi8 (Leica) using bright field objective at 20x at $0.5-6$ frames per second.

2.1.2 Image segmentation. Image segmentation is done using standard Matlab functions for the image processing. First, the image is thresholded using tne `edge` function in two steps: the automatic threshold is identified and then lowered to achieve better edge detection. The detected edges are dilated using the `imdilate` function. Then, the closed areas are filled with the `imfill` function to remove black spots inside detected cells. Finally, `bwareaopen` is used to remove small noise. The result is a mask that selects only regions occupied by algae.

2.1.3 Particle image velocimetry (PIV). The measurements of the velocity and vorticity fields were done using the `PIVlab` app for Matlab[22]. The method is based on the comparison of the intensity fields of two consequent photographs of algae. The difference in the intensity is converted into velocity field measured in px/frame and then converted to μm/h[23]. To avoid spurious noise PIV was applied after image segmentation only to the regions occupied by algae.

2.1.4 Cell tracking. The tracking and motion analysis of algae in 2D is performed using Trackpy: a particle-tracking Toolkit written in Python, available at `https://zenodo.org/record/3492186`. The original implementation of the tracking algorithm is reported in Ref.[24]. The first step of the tracking consists in the location of the algae in each image to extract their coordinates. For this purpose we set the function `locate`, performing a band pass and threshold, with the following parameters: diameter =17, minmass=10^5, separation=5, invert=True. The function `annotate` allows the direct visualization of the detected particles. Afterwards, the algorithm links the coordinates in time to extract the trajectories (function `link` with parameters: search range=3, memory=5). The drift motion is then computed and subtracted away (`compute_drift` function) and the final trajectories are obtained. The trajectories are analyzed with the `emsd` function to compute the ensemble mean square displacement (MSD) of all particles.

2.2 Simulations

2.2.1 Model for interacting 2D active disks. We performed Molecular Dynamics simulations of a system made of active self-rotating particles using LAMMPS (Large-scale Atomic/Molecular Massively Parallel Simulator)[21]. Each particle (described as a 2D disk) has the following physical properties:

- it is an active particle and it has the ability of both self propel to move in a straight direction and to self-rotate around its center
- it is moving on a viscous medium, so performing a Brownian motion
- the system is made up of particles with two different radii in order to avoid crystallization
- it interacts with its nearest neighbor particles via a granular potential (Hertzian potential) to which we add an adhesion term (Derjagun-Muller-Toporov Model[25]). This is done in order to take into account the adhesion properties of cells.

The equations of motion describing the center of mass position $\overrightarrow{x}_i(t)$ and the rotational angle $\theta_i(t)$ of the two-dimensional disk i at time t are given by

$$\frac{d^2\overrightarrow{x}_i(t)}{dt^2}=\frac{1}{m}[\overrightarrow{\Gamma}_i(t)+\overrightarrow{\chi}_i(t)+\overrightarrow{\Phi}_i(t)+\sum_{n.n.}\overrightarrow{\Psi}^n_{ij}(t)+\sum_{n.n.}\overrightarrow{\Lambda}_{ij}(t)] \quad (1)$$

$$\frac{d^2\theta_i(t)}{dt^2} = \frac{1}{I_z}[\Upsilon_i(t) + \Theta_i(t) + \tau_z{}^i(t) - \sum_{n.n.}(\overrightarrow{R}_i \times \overrightarrow{\Psi}^t_{ij}(t))_z] \quad (2)$$

Here the sums are over the nearest neighbor (n.n) disks and $\overrightarrow{R}_i$ is a vector normal to the disk surface and of amplitude equal to the disk radius. The quantities are dimensionless because units are set to Lennard-Jones units in LAMMPS. It is, however, always possible to convert to real units by setting the disk radius to the typical algae radius. Since particles are moving in a viscous environment, the term $\overrightarrow{\Gamma}_i(t)$ takes into account the friction due to the surrounding medium. Its value is:

$$\overrightarrow{\Gamma}_i(t) = -\frac{m}{\beta}\overrightarrow{v}(t) \quad (3)$$

As we can see this term is proportional to the linear velocity $\overrightarrow{v}(t)$ of the particle and to the particle mass m. Here, the input parameter β is inversely proportional to the fluid viscosity. Since cells moving in a medium are usually in an overdamped regime, we set $\beta = 0.1$ so that Brownian dynamics can effectively be considered as an overdamped Langevin dynamics. Friction enters also in the rotational motion of our $2D$ disks, since we have a friction term proportional to the angular velocity and to the moment of inertia of the disks I given by

$$\Upsilon_i(t) = -\frac{10}{3}\frac{I}{\beta}\omega(t) \quad (4)$$

Next, we consider in Eqs. 1 and 2 a term representing random noise, described by $\overrightarrow{\chi}_i(t)$ and $\Theta_i(t)$. From the fluctuation/dissipation theorem, the magnitude of $\overrightarrow{\chi}_i(t)$ is proportional to $\sqrt{\frac{K_b T m}{dt\beta}}$, where K_b is the Boltzmann constant, T is the temperature, m is the mass of the particle, dt is the timestep, and β is the damping factor. In the case of $\Theta_i(t)$, the mass in the previous equation is substituted by the moment of inertia I. The random noise is uncorrelated with $\langle\xi(t)\rangle = 0$ and $\langle\xi(t)\xi(t')\rangle \propto \delta(t-t')$.

Since our aim is to describe active particles, we include in Eq. 1 and Eq. 2 terms taking into account the ability of the particle to self sustain its motion. The term $\overrightarrow{\Phi}_i(t)$ takes into account the ability of the cell to self-propel. The biological mechanisms that allow the cell to move are simply modeled as a force with a constant modulus pointing in the direction in which the particle was already moving, considering a characteristic time until the particle can change direction

$$\overrightarrow{\Phi}_i(t) = V\frac{\overrightarrow{v}(t)}{|v|} \quad (5)$$

The term $\overrightarrow{\tau}^i_z(t)$ takes into account the self-rotation of the particle adding a constant torque along the $\hat{z}$ direction at each time step for each particle. Since at the beginning of the simulation, particles are endowed with an initial angular velocity, either clockwise or counter-clockwise, the torque term initially follows the direction of rotation, so that a particles that moves clockwise at the beginning continues to rotate in that direction under the self rotation effect. Of course changes of rotation direction can arise due to interaction among particles. In order to study the effect of rotation on the collective properties of our system, we performed simulations for different values of the active torque τ_z. The term $\overrightarrow{\Psi}_{ij}(t)$ describes contact interactions between the particles, according to the Hertzian model[26,27]. In particular the form of the force is:

$$\begin{aligned}\overrightarrow{\Psi}_{ij}(t) = &\sqrt{\delta}\sqrt{\frac{R_i R_j}{R_i + R_j}}[(k_n\delta\hat{n}_{ij} - m_{eff}\gamma_n\overrightarrow{v}_n) + \\ &- (k_t\overrightarrow{\Delta s_t} + m_{eff}\gamma_t\overrightarrow{v}_t)]\end{aligned} \quad (6)$$

Where R_i and R_j are the radii of the interacting disks. In our simulations, disks have two different radii $R_1 = 1.96$ and $R_2 = 1.4$, in order to avoid crystallization. The force is divided in two components, the force that is normal to the contact surface between the two particles and the one that is tangential. The normal force has two terms, a contact force and a damping force. Here δ is the overlap distance between two particles, k_n is the elastic constant for the normal contact, $\hat{n}_{ij}$ is the unit vector along the line connecting the centers of the two interacting disks, γ_n is the viscoelastic damping constant for normal contact and $\overrightarrow{v}_n$ is the normal component of the relative velocity of the two particles. This component of the force enters in Eq. 1, influencing the equation of motion of the center of mass of the disk. The tangential force also has two terms: a shear force and a damping force. The shear force contains a "history" effect that accounts for the tangential displacement between the particles for the duration of the time they are in contact. Here k_t is the elastic constant for tangential contact and $\overrightarrow{\Delta s_t}$ is the tangential displacement vector between two particles. In the tangential damping force the term γ_t is the viscoelastic damping constant for tangential contact and $\overrightarrow{v}_t$ is the tangential component of the relative velocity of the two particles. This tangential component of the Hertzian interaction enters in the rotational equation of motion, via the torque $-\overrightarrow{R}_i \times \overrightarrow{\Psi}^t_{ij}(t)$.

Then, in order to study the role of adhesion between particles, typical of many biological systems, a term taking into account the adhesion is inserted in Eq. 1. This is done using the Derjaguin-Muller-Toporov model[25,28], where the adhesive force has the form $\overrightarrow{\Lambda}_{ij}(t) = -\frac{A_{cc}R_{ij}\hat{n}_{ij}}{6\varepsilon^2}$, where A_{cc} is the Hamaker constant that takes into account the coefficient of the particle-particle pair interaction, $R_{ij} = \frac{R_i R_j}{R_i + R_j}$ is the effective radius of the two touching particles and ε is the least possible spacing between the contact surfaces. In particular the adhesion force is calculated in the LAMMPS code `pair-dmt` distinguishing between two cases: If the distance among the centers of two spheres is bigger than the sum

of the radii $r > R_1 + R_2$, the adhesion force takes the form $\overrightarrow{\Lambda}_{ij}(t) = -\frac{A_{cc}R_{ij}\hat{n}_{ij}}{6[r-(R_i+R_j)+\varepsilon]^2}$, otherwise the adhesion force becomes $\overrightarrow{\Lambda}_{ij}(t) = -\frac{A_{cc}R_{ij}\hat{n}_{ij}}{6\varepsilon^2}$. So the adhesion is simply represented by a spring force when two particles overlap. In the following we studied the role of adhesion performing simulations with different values of the Hamaker constant A_{cc}. Integrating Eqs. 1 and 2, it is possible to update positions and velocities of the particles at each time step of our simulation.

2.2.2 Parameters used for the simulations. For the simulations we used 2D disks of radius $R_1 = 1.96$ and $R_2 = 1.4$ and density of the disk $d = 0.46$ (so mass $m = d * \pi R^2$). We used a time step of 0.0001 in LJ units and run the simulations for 10^6 steps, so covering 100 time units. The temperature is constant during the integration of the equation of motion and equal to $T = 1$.

3 Results

3.1 Active rotators in the diluted limit

To quantify self-rotation in *C. reinhardtii*, we first consider the diluted limit shown in Fig. 1a and perform a PIV analysis to recostruct the probability distributions for linear and angular velocities (also reported in Fig. 1a). The plots show that the distributions of the absolute value of the linear velocities follows a Rayleigh-like distribution, while the angular velocity distribution has a Gaussian-like behavior. When algae are stressed by adding 150*mM* NaCl added to the medium, we observe the formation of rotating clusters because these algae tend to aggregate in response to stress. The probability distributions obtained under stress indicate that aggregation leads to a decrease of velocity and angular velocity fluctuations.

In order to explain these experimental observations and gain insight on those systems of active rotators, we perform simulations in LAMMPS using the model described in the model section. We consider a low density system with a packing fraction $\phi = \frac{V_{particles}}{V_{TOT.}} = 0.14$ and active torque $\tau_z = 6000$. When adhesion is switched off ($A_{cc} = 0$), the active particles do not form clusters and rotate mostly individually (see Fig. 1b). When adhesion is present, however, particles aggregate into clusters as shown in Fig. 1b (obtained for $A_{cc} = 3950$).

From the simulations, we also extracted the probability distributions for the linear and angular velocities of the particles, in the cases with and without adhesion (see Fig. 1b). The distributions obtained from the model are very similar to those observed in experiments, suggesting that our model can capture some important features of those biological systems.

3.2 Active rotators in the dense regime

After comparing model and experiments in the dilute regime, we investigate how the self-rotation of the disks can affect the phase behavior of a dense system of interacting rotators. We first analyze with PIV the motion of *C. reinhardtii* at higher densities and find that increasing the density, the algae became more motile, since the linear velocity peak is shifted toward higher values and the variance of the angular velocity distribution increases (compare the distributions in Fig 1a and Fig. 2a). Visual inspection of the velocity and vorticity maps obtained by PIV shows that algae rotate and tend to form rotating clusters and vortex like behavior. The experimental observation that increasing the density leads to higher mobility can not easily be explained by the model. If we only increase the density, keeping all the other parameters constant, the mobility progressively decreases until the system jams. This is the typical behavior expected for inactive jamming phenomena [18]. In this active system, however, a possible explanation is that algae respond to crowding by increasing their active torque. We therefore study numerically the effect of self-rotation in a dense system of active rotators.

To improve the statistics, our numerical results are averaged over ten initial configurations initially placed into a jammed phase. To this, end we create a simulation box with 1000 disks in random positions (500 with radius $R_1 = 1.96$ and 500 with radius $R_2 = 1.4$, corresponding to a binary mixture with diameter ratio of 1.4, as in previous studies on jamming of a 2D disk packing [29,30]). We then performed subsequent steps of box reduction and energy minimization, monitoring the behavior of the pressure of the system as a function of the packing fraction ϕ.

It is already known from previous studies on random packing of frictionless particles that ϕ at which the pressure becomes non zero is the same as the jamming threshold, when also the static shear modulus becomes non-zero [29]. This can be understood by thinking that when the packing fraction is small, particles do not touch and the internal pressure is zero. Increasing the particle density via box reduction, the system reaches a state in which the particles touch and are blocked into a rigid structure. At this point, a further increase of the packing fraction will lead to a pressure increase. Hence, pressure is a good indicator of the jamming point.

In our case, we observe that the pressure is zero until $\phi \simeq 0.78$ and increasing rapidly for larger values of ϕ. To ensure that the system is in the jammed state, we chose initial configurations with $\phi = 0.87$. Previous work on packing and jamming of 2D bidisperse hard disks at $T = 0$ shows that the value for random close packing ϕ_{RCP} (maximum density without crystallization) is $\phi = 0.84$ [30]. Here, we are considering friction so that jamming is reached at a density lower than ϕ_{RCP}. Furthermore, we are considering a system that is

not at zero temperature. Thus as suggested by the jamming diagram proposed by Liu e Nagel[18], the jamming transition is expected to occur at a higher density. These facts justify the value we found for the onset of jamming. It has recently been observed that the critical value of the density at which the jamming transition takes place can depend also on the conditions in which the system has been prepared and varies also within the same material[31] making it hard to find a well defined value of the packing fraction for the onset of jamming. Furthermore, we have to consider that our 2D disks are not hard, their 'hardness' being controlled by the k_n coefficient in the Hertzian potential. Thus, they can overlap and elastically deform, reaching higher values of packing fractions.

We perform MD simulations starting from the initial jammed configurations and increasing the value of the active torque τ_z. When self-propulsion is switched off ($v = 0$) as well as the adhesion term ($A_{cc} = 0$), we noticed that at low active torques the system stays in a jammed phase, characterized by a very low mobility of the active disks. Above a critical value of the active torque, the system switches to a flowing, unjammed phase, characterized by a high mobility of the disks. Fig. 2b reports typical snapshots of the simulations for different values of the active torque, highlighting the internal rotations of the disks. We then analyzed the probability distribution of linear and angular velocities and, as shown in Fig. 2b, we observe that disks increase their velocities in response to the active torque. The distribution of the linear velocities is qualitatively similar to the experimentally measured one (Fig. 2a) while the distribution of angular velocity displays two peaks, reflecting the constant active torque used in the simulations. The active torque in algae is likely not constant explaining the difference between simulations and experiments.

3.3 Rotational induced unjamming transition

To gain insight on the mobilization of the jammed active disks, we studied individual trajectories of the disks computing their mean square displacement (MSD). We first consider the experimental data and perform tracking of individual algae. Fig. 3a reports an example of the recorded trajectories which displays a diffusive behavior as show in Fig. 3b.

We then perform a similar analysis on the simulations and in Fig. 3c, we show that in the jammed phase trajectories are localized (see inset of Fig. 3c) while for higher values of the active torque they spread. The mean square displacement is close to zero for low torques while it grows linearly for larger values of the self-rotation (Fig. 3d and Fig. 3e). From a linear fit of the long time region of the MSD, we also extracted an effective diffusion coefficient, that clearly shows a sharp increase at ($\tau_z = 4000$), suggestive of a phase transition into a flowing state (Fig. 3f).

Since we have seen that the self-rotation can lead from a jammed to an unjammed state, it is interesting to investigate the role of adhesion, present in many cellular systems, including *C. reinhardtii* where it could be triggered by stress. As discussed in the Model section, adhesion is modeled using the Derjaguin-Muller-Toporov model and the parameter used to tune the intensity of the adhesion force in the simulations is the Hamaker constant A_{cc}. We performed simulation with $\tau_z = 6000$, so in the unjammed phase switching on the adhesion term. Analyzing the mean square displacement and as before the effective diffusion coefficient, it emerges that increasing the adhesion strength the system remains unjammed until a critical value ($A_{cc} \sim 1500 - 2000$) at which diffusion is strongly reduced, unveiling a transition to a jammed phase.

3.4 Self-rotation and self-propulsion

We next consider the interplay between self-propulsion and self-rotation, exploring the behavior of the system in terms of two parameters τ_z, the active torque and v, the self-propulsion. We consider a system of disks placed at the jamming density ($\phi = 0.87$) without adhesion. We scan the parameter space and record the trajectories of disks. We then compute the mean-square displacement and estimate the effective diffusion constant D_{eff} for each case.

Fig. 5a reports the variation of diffusion constant as a function of the active torque in presence of a relatively weak self-propulsion $v = 25$. The curve shows that increasing self-rotation leads to a rapid reduction of diffusion. Further increase in the self-rotation, however, induces an increase in the diffusion. This monotonic behavior is due to the fact that in absence of self-rotation, self-propulsion leads to coherent directed motion. We have checked that this coherent motion is not an artifact of periodic boundary conditions, but persists also for closed boundary conditions. Self-rotation breaks the coherence of the self-propelled motion, inducing jamming. Rotational-induced unjamming is then observed for higher values of the active torque. In absence of self-rotation, unjamming is driven by self-propulsion as already observed in many active particle models (see Fig. 5b). All the numerical simulations can then be summarized into a qualitative phase-diagram reported in Fig 5c, where we plot the effective diffusion constant as a function of V and τ_z.

4 Discussion

Our work was inspired by the observation of a natural example of active rotators like *C. reinhardtii*. Quantification by image segmentation and PIV analysis shows that this kind of algae can not only self-rotate[13] but also aggregate forming collectively rotating clusters. The formation of these aggregates is observed both in high density limit, and low density in presence of a stress agent, such as NaCl. Starting from these sim-

ple observations, we built and simulate a model of 2D active disks that have the ability to self-rotate and interact with each other. We found that in the low density limit ($\phi = 0.14$) and in presence of an adhesion term among the disks, the active rotators tend to aggregate and form rotating clusters, in analogy with what is observed in algae. Similar rotating clusters where observed in confined cellular assemblies in vitro [32] and is glandular tissues [33], as well as in previous simulations of a model of self-propelled particles [34]. In particular, we saw that the adhesion term plays a crucial role in the formation of clusters, suggesting that a form of attraction should also be present in the case of *C. reinhardtii*.

An interesting feature of the clusters is that they rotate collectively but also show internal particle rotations that are not always synchronized with the global rotation of the cluster. A similar behavior is observed in *C. reinhardtii* and also in previous studies on 2D active spinners embedded in passive colloidal monolayers [14]. In the latter case, it has been observed that the presence of a passive monolayer that behaves elastically as a solid-like material, induces an attractive interaction between the active rotating particles, which results in aggregation of spinners [14]. We also mention here another related experiment where an active granular material composed of spinning disks is confined within a circular arena [35]. The authors reveal an interesting transition in the collective circulation of the spinning disks [35].

Furthermore, we studied with our simulations the role of self-rotation in a jammed system. We observed that self-rotation alone can lead to a phase transition from a jammed solid-like state to an unjammed, flowing phase. In the past the role of active forces has been investigated, studying the phase diagram of 2D soft disks, that exhibit a liquid phase with giant number fluctuations at low packing fraction ϕ and high self-propulsion V and a jammed phase at high ϕ and low V [36] or in active dumbbell systems with different packing fraction and Péclet number [12]. These studies, however, did not consider self-rotations as we did. We also studied the effect of adhesion and investigated its role when combined to the self-rotation of the disks. We revealed how adhesion can act in the opposite direction with respect to self-rotation, promoting jamming. Increasing the adhesion strength, we can move the system from a flowing unjammed phase to a jammed one. It would be interesting to observe a similar phase transition in experiments controlling self-rotation and adhesion, for instance in chiral ative fluids made of superparamagnetic particles in a magnetic field [14]).

A better characterization of the key features of this jamming-unjamming transition in active particles systems could be very useful to better understand biological processes in which the involved cells have the ability to self-rotate, both at a single particle level or as collective rotation. For example, experiments involving epithelial cells confined in narrow channels showed the formation of vorticity, suggesting a possible role for rotations in collective cell migration [37]. Another context in which the mechanical properties of tissues gain a peculiar interest is in the study of cancer cells, and in particular in the formation of metastasis. It has been observed that cancer cells are softer than non-cancerous ones [38], divide more often than healthy cells and, as in the case of the epithelial-to mesenchymal transition (EMT), they decrease the cell-cell adhesion, potentially allowing for rotational motion. All those features contribute to fluidize a confluent tissue of cancer cells, favoring the unjamming transition and so the formation of diffusing groups of cells (for a review see [39]). Hence, our theoretical study of a model system of active rotators reveals how self-rotation of the active particles is a parameter that can control the jamming-unjamming transition, besides already well studied mechanisms such as self-propulsion [36] or density, and can help in better understanding physical aspects of cancer cell invasion [40].

Acknowledgements

SZ thanks the Alexander von Humboldt foundation for the Humboldt Research Award for support and Ludwig-Maximilian University and Friedrich-Alexander-Universität Erlangen-Nürnberg for hospitality. CAMLP thanks Ludwig-Maximilian University for hospitality.

References

1 M. C. Marchetti, J.-F. Joanny, S. Ramaswamy, T. B. Liverpool, J. Prost, M. Rao and R. A. Simha, *Reviews of Modern Physics*, 2013, **85**, 1143.
2 S. Ramaswamy, *Annu. Rev. Condens. Matter Phys.*, 2010, **1**, 323–345.
3 A. Cavagna and I. Giardina, *Annu. Rev. Condens. Matter Phys.*, 2014, **5**, 183–207.
4 D. Needleman and Z. Dogic, *Nature Reviews Materials*, 2017, **2**, 1–14.
5 A. Z̀ottl and H. Stark, *Journal of Physics: Condensed Matter*, 2016, **28**, 253001.
6 H.-R. Jiang, N. Yoshinaga and M. Sano, *Physical Review Letters*, 2010, **105**, 268302.
7 B. Dai, J. Wang, Z. Xiong, X. Zhan, W. Dai, C.-C. Li, S.-P. Feng and J. Tang, *Nature nanotechnology*, 2016, **11**, 1087.
8 A. Bricard, J.-B. Caussin, D. Das, C. Savoie, V. Chikkadi, K. Shitara, O. Chepizhko, F. Peruani, D. Saintillan and D. Bartolo, *Nature communications*, 2015, **6**, 1–8.
9 D. Levis and L. Berthier, *Physical Review E*, 2014, **89**, 062301.
10 C. Bechinger, R. Di Leonardo, H. Löwen, C. Reichhardt,

G. Volpe and G. Volpe, *Reviews of Modern Physics*, 2016, **88**, 045006.
11 P. Digregorio, D. Levis, A. Suma, L. F. Cugliandolo, G. Gonnella and I. Pagonabarraga, *Physical Review Letters*, 2018, **121**, 098003.
12 L. F. Cugliandolo, P. Digregorio, G. Gonnella and A. Suma, *Physical Review Letters*, 2017, **119**, 268002.
13 S. K. Choudhary, A. Baskaran and P. Sharma, *Biophysical journal*, 2019, **117**, 1508–1513.
14 J. L. Aragones, J. P. Steimel and A. Alexander-Katz, *Soft matter*, 2019, **15**, 3929–3937.
15 D. Banerjee, A. Souslov, A. G. Abanov and V. Vitelli, *Nature communications*, 2017, **8**, 1–12.
16 G. Kokot, S. Das, R. G. Winkler, G. Gompper, I. S. Aranson and A. Snezhko, *Proceedings of the National Academy of Sciences*, 2017, **114**, 12870–12875.
17 S. Farhadi, S. Machaca, J. Aird, B. O. T. Maldonado, S. Davis, P. E. Arratia and D. J. Durian, *Soft matter*, 2018, **14**, 5588–5594.
18 A. J. Liu and S. R. Nagel, *Nature*, 1998, **396**, 21–22.
19 J.-A. Park, J. H. Kim, D. Bi, J. A. Mitchel, N. T. Qazvini, K. Tantisira, C. Y. Park, M. McGill, S.-H. Kim, B. Gweon *et al.*, *Nature materials*, 2015, **14**, 1040–1048.
20 O. Chepizhko, M. C. Lionetti, C. Malinverno, C. Giampietro, G. Scita, S. Zapperi and C. A. La Porta, *Soft matter*, 2018, **14**, 3774–3782.
21 S. Plimpton, *Fast parallel algorithms for short-range molecular dynamics*, Sandia national labs., albuquerque, nm (united states) technical report, 1993.
22 W. Thielicke and E. Stamhuis, *Journal of Open Research Software*, 2014, **2**, e30.
23 O. Chepizhko, C. Giampietro, E. Mastrapasqua, M. Nourazar, M. Ascagni, M. Sugni, U. Fascio, L. Leggio, C. Malinverno, G. Scita *et al.*, *Proceedings of the National Academy of Sciences*, 2016, **113**, 11408–11413.
24 J. C. Crocker and D. G. Grier, *Journal of colloid and interface science*, 1996, **179**, 298–310.
25 B. V. Derjaguin, V. M. Muller and Y. P. Toporov, *Journal of Colloid and interface science*, 1975, **53**, 314–326.
26 N. V. Brilliantov, F. Spahn, J.-M. Hertzsch and T. Pöschel, *Physical review E*, 1996, **53**, 5382.
27 L. E. Silbert, D. Ertaş, G. S. Grest, T. C. Halsey, D. Levine and S. J. Plimpton, *Physical Review E*, 2001, **64**, 051302.
28 E. Barthel, *Journal of Physics D: Applied Physics*, 2008, **41**, 163001.
29 C. S. O'Hern, S. A. Langer, A. J. Liu and S. R. Nagel, *Physical Review Letters*, 2002, **88**, 075507.
30 C. S. O'hern, L. E. Silbert, A. J. Liu and S. R. Nagel, *Physical Review E*, 2003, **68**, 011306.
31 N. Kumar and S. Luding, *Granular Matter*, 2016, **18**, 58.
32 F. J. Segerer, F. Thüroff, A. Piera Alberola, E. Frey and J. O. Rädler, *Physical Review Letters*, 2015, **114**, 228102.
33 K. Tanner, H. Mori, R. Mroue, A. Bruni-Cardoso and M. J. Bissell, *Proceedings of the National Academy of Sciences*, 2012, **109**, 1973–1978.
34 H. Levine, W.-J. Rappel and I. Cohen, *Physical Review E*, 2000, **63**, 017101.
35 M. Workamp, G. Ramirez, K. E. Daniels and J. A. Dijksman, *Soft matter*, 2018, **14**, 5572–5580.
36 S. Henkes, Y. Fily and M. C. Marchetti, *Physical Review E*, 2011, **84**, 040301.
37 S. R. K. Vedula, M. C. Leong, T. L. Lai, P. Hersen, A. J. Kabla, C. T. Lim and B. Ladoux, *Proceedings of the National Academy of Sciences*, 2012, **109**, 12974–12979.
38 L. Oswald, S. Grosser, D. M. Smith and J. A. Käs, *Journal of physics D: Applied physics*, 2017, **50**, 483001.
39 C. A. La Porta and S. Zapperi, *Cell Migrations: Causes and Functions*, Springer, 2019, vol. 1146.
40 C. A. La Porta and S. Zapperi, *The physics of cancer*, Cambridge University Press, 2017.

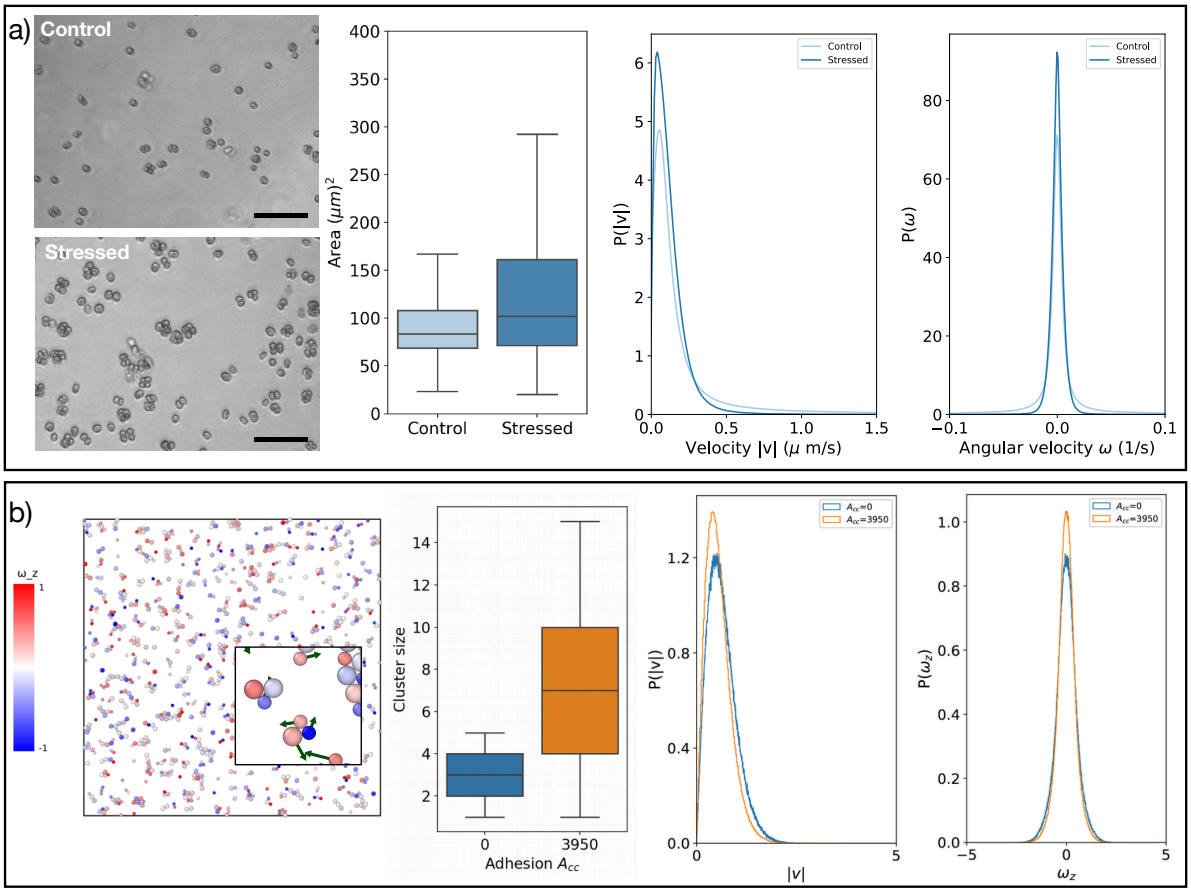

Fig. 1 a) Typical snapshots of *C. reinhardtii* suspensions (scale bars 50μm) at low density with and without the stress induced by the presence of NaCl are shown together with a boxplot of cluster areas, the distribution the absolute value of the linear velocities $P(|v|)$ and the distribution of the angular velocities $P(\omega)$. b) Snapshots of the simulations at low density $\phi = 0.14$ in presence of active torque ($\tau_z = 10$) with adhesion ($A_{cc} = 3950$). Particles are colored according to their angular velocity ω_z. The formation of clusters is clearly visible. In the inset a zoom of a portion of the simulated box is shown, together with the velocity vectors of the particles. In particular it is easy to see a system of three collectively rotating particles. We also show a boxplot of cluster sizes and the distributions of velocities and angular velocities with and without adhesion.

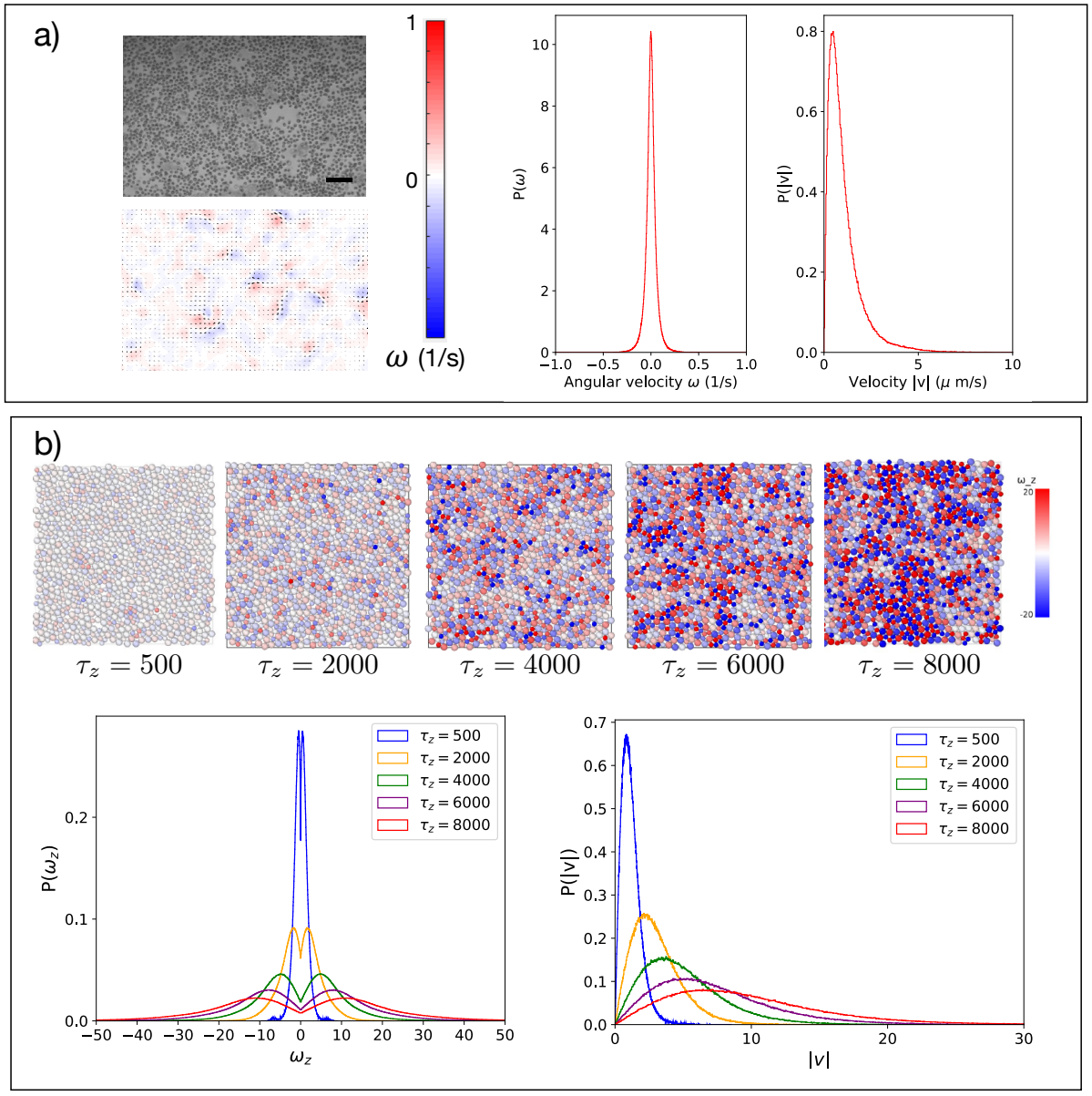

Fig. 2 a) Typical snapshot of a *C. reinhardtii* suspension at high density (scale bars 100μm) is shown together with the corresponding map of angular velocities obtained by PIV. On the right-hand side, we report plots of the probability distribution of the angular velocity $P(\omega)$ and of the absolute value of the linear velocity $P(|v|)$. b) Typical snapshot of the system obtained with the model at high density for different values of the active torque. Below we report the corresponding distributions of angular and linear velocities.

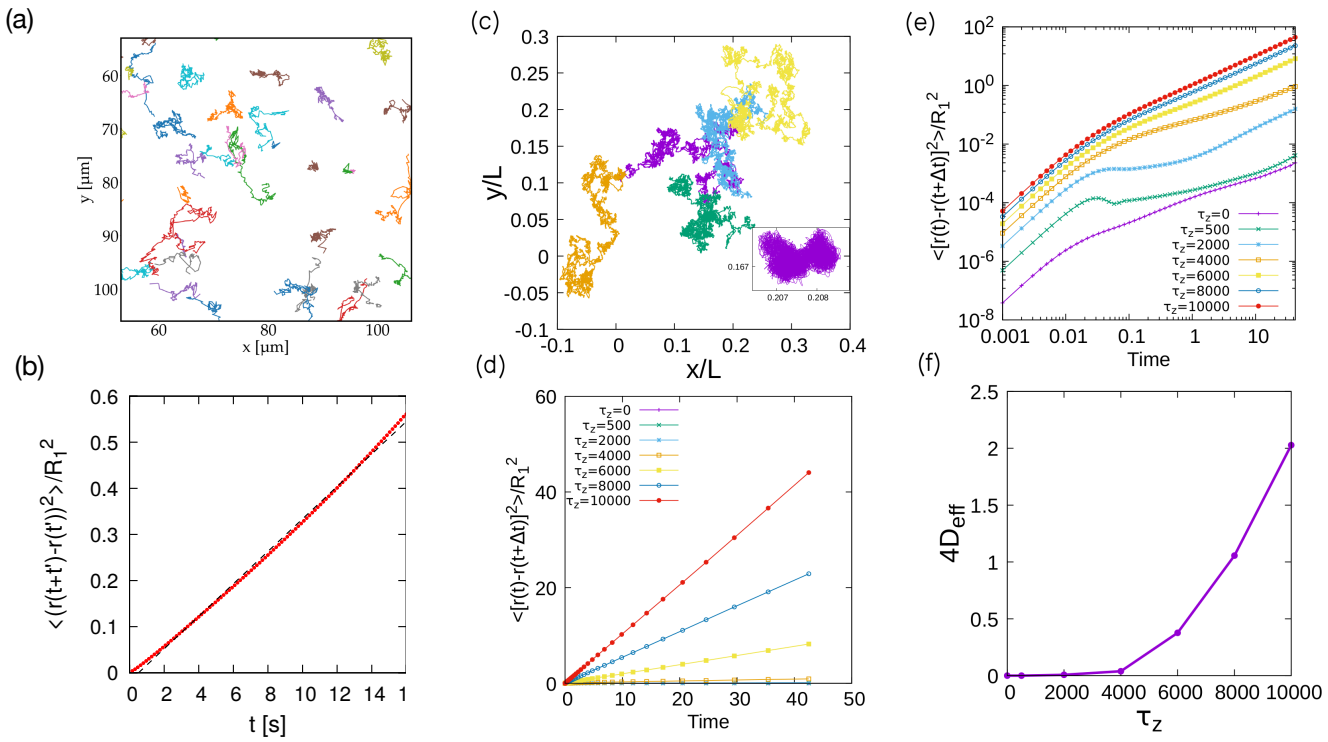

Fig. 3 a) Trajectories of randomly selected algae for experimental conditions similar to those reported in Fig. 2a. b) Mean-square displacement of the experimental trajectories, showing diffusive behavior. c) Selected trajectories obtained in simulations for the system in the jammed phase ($\tau_z = 500$ in the inset) and in the system in the unjammed phase ($\tau_z = 8000$, main plot). In both plots, the the coordinates are rescaled using the length of the simulation box L. d) The time evolution of the mean-square displacement averaged over all the disks belonging to the system is shown for different values of the active torque, showing a clear increase for increasing values of the disks self rotation. e) The same plot as in d) is reported also in logarithmic scale. f) The diffusion coefficient, obtained from a linear fit of the long time region of the mean square displacement is plotted. The increase after a critical value of the active torque τ_z is associated to a phase transition from a jammed/solid-like phase to an unjammed/flowing phase of the system.

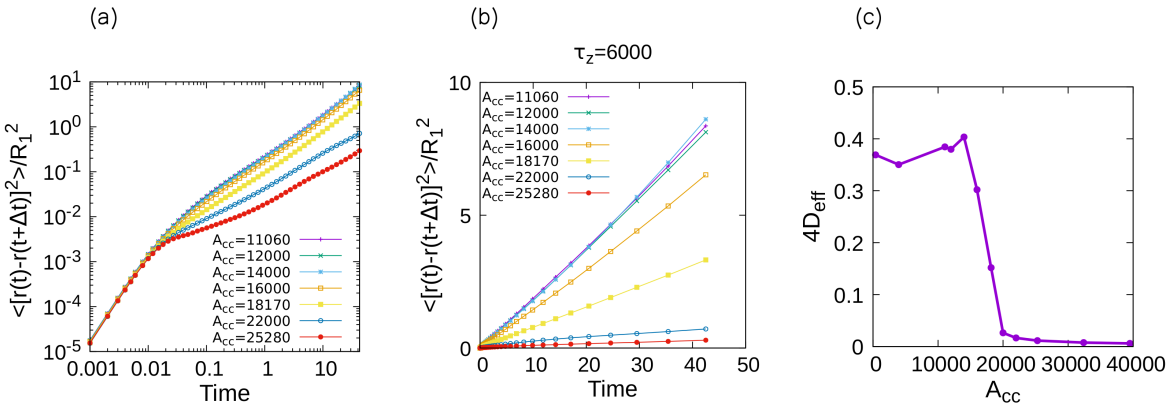

Fig. 4 The mean square displacement of the system in the unjammed phase ($\tau_z = 6000$) and high density ($\phi = 0.87$) is shown for different values of the Hamaker constant A_{cc}, that defines the intensity of the adhesive potential among the particles. Results are reported in a) logarithmic and b) linear plots. Increasing the strength of the adhesion, the mean square displacement decreases. c) The effective diffusion coefficient averaged on all the disks is extracted from the linear fit of the mean square displacement. Here the phase transition from the unjammed to the the jammed phase is clearly visible as the diffusion coefficient rapidly drops to zero for large adhesion strengths.

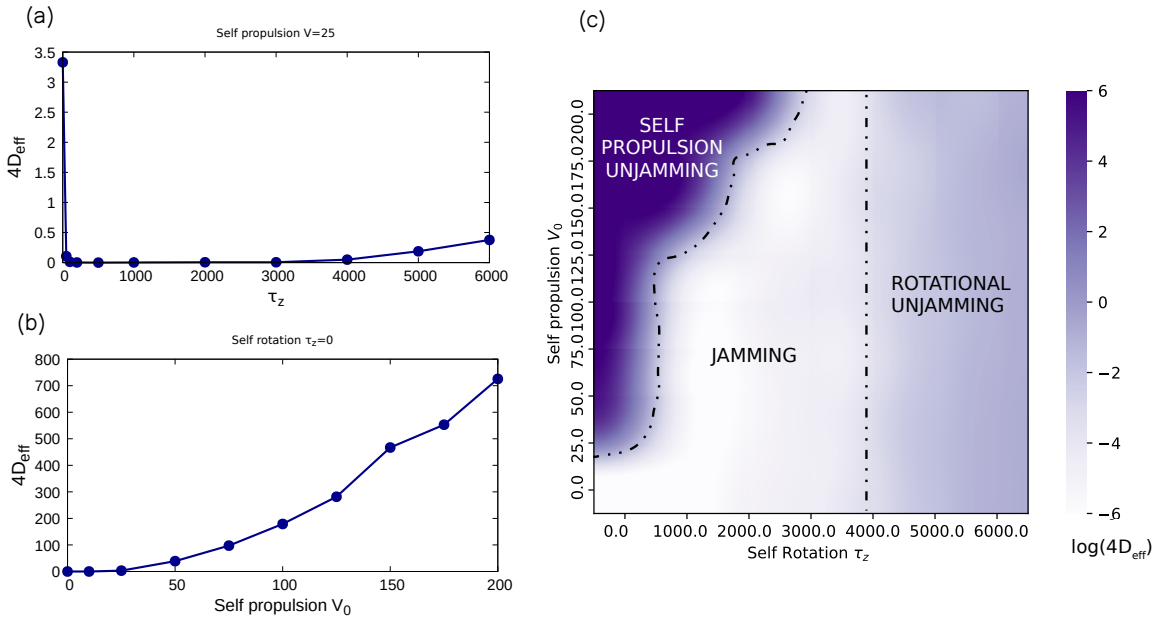

Fig. 5 The effective diffusion constant D_{eff} as a function of a) active torque τ_z at constant self-propulsion $V = 25$ and b) self-propulsion V at $\tau_z = 0$. c) A qualitative phase diagram can be obtained by plotting $\log D_{eff}$ as a function of V and τ_z. Notice the peculiar role of the self-rotation that can both induce jamming and unjamming, depending on the presence of self-propulsion. The color plot is obtained by interpolating the estimated values of $\log 4D_{eff}$.